Understanding heterogeneity in discontinuous compression moulded composite materials for high-volume applications

D. J. Bull[1], J. M. Dulieu-Barton[2], O. T. Thomsen[1]

[1]Infrastructure Research Group, Faculty of Engineering and the Environment, University of Southampton, UK
[2]Engineering Materials Research Group, Faculty of Engineering and the Environment, University of Southampton, UK

ABSTRACT

To understand the mechanisms contributing to material heterogeneity in discontinuous compression moulded composite materials, a data rich study combining digital image correlation (DIC), thermoelastic stress analysis (TSA) and X-ray computed tomography (CT) is presented. Initial results show that DIC and TSA are capable of capturing variability in surface strains and stresses when subjected to a cyclic load, and X-ray CT has been used to quantify volumetric variability in local resin volume content and distribution of local fibre orientations, which all contribute to the complex response detected on the component surface.

Keywords: Lock-in digital image correlation, thermoelastic stress analysis, X-ray computed tomography, carbon fibre composite materials, complex materials

Materials and methods

Discontinuous compression moulded composite materials offer advantages in reducing manufacturing costs and high-speed manufacture of composite components with the capability of producing components in less than 5 minutes as required for high volume manufacturing of e.g. automotive components with annual production numbers of 100,000 or more. However, a significant limitation is the heterogeneous mechanical properties at the mesoscale which adds complications to predicting the mechanical behaviour and thereby potentially reducing the uptake in the composite industry. To reduce the level of variability of properties it is important to understand how the manufacturing process may affect the material performance.

A compression moulded carbon fibre epoxy composite test coupon comprising of random orientated chopped fibres [1] was manufactured with dimensions of 400 x 50 x 3.8 mm. To study the component's mechanical response under loading, two full-field imaging techniques were employed: thermoelastic stress analysis (TSA) [2] and lock-in digital image correlation (LIDIC) [3]. A uniaxial cyclic load was applied to the specimen with a mean load of 9 kN and an amplitude of 7 kN at a frequency of 10 Hz. To complement the surface stress and strain observations from TSA and LIDIC, X-ray computed tomography (CT) was conducted to generate a detailed quantification of the local resin rich regions and local fibre orientations both on the surface and within the bulk.

The TSA technique records small temperature changes corresponding to changes in stress. When coupled with a sinusoidal cyclic load, it is possible to apply a lock-in algorithm which can reconstruct the amplitude of temperature change (ΔT). The relationship between the change in temperature, ΔT, and the sum of principal stresses, $(\sigma_{11} + \sigma_{22})$, (assuming adiabatic conditions) is as follows[2]:

$$\Delta T = -\frac{T}{\rho C_p}\Delta(\alpha_1\sigma_{11} + \alpha_2\sigma_{22}) \quad (1)$$

where the parameters T, ρ, Cp and α denote the reference absolute temperature, density, specific heat capacity at constant pressure and α is the coefficient of linear thermal expansion respectively.

The LIDIC approach [3] extends the traditional digital image correlation (DIC) technique with a lock-in algorithm to capture the amplitude of strains on a cyclic load. A stereo setup was used using two cameras to track a black and white speckle pattern applied to the material's surface. Due to limitations of camera bandwidth, the images were captured at a frame rate of 1.95 Hz and hence were undersampled. However, by capturing over many cycles (100 frames) and applying a lock-in algorithm, the full-field amplitude of strain can be calculated [3].

Results and analysis

To fully appreciate the heterogeneity of the compression moulded component, for each of the three techniques the data was aligned and a sample of the image data was taken from 10 subsets (each 10 mm x 10 mm), as shown Figure 1 for (a) X-ray CT, (b) LIDIC and (c) TSA data. The local fibre orientation was quantified along the through-thickness direction on each subset using the directionality plugin in ImageJ applying the Fourier components method. Resin area fraction on the surface and through the volume of each subset was quantified by measuring the segmented porosity features (by global thresholding) against the total area or volume respectively. The average change in strain and ΔT values obtained for each subset were normalised with the overall values from the entire field of view of the test specimen and are indicated in Figure 1 for each subset. It is clear from the observed data that the local fibre orientation and resin area fraction are highly variable subset by subset. These surface variations are not reflected by changes in strain and ΔT value.

If the strains in the x-direction and the y-direction (perpendicular and parallel to loading direction respectively) are added and normalised by the global average of the sum of the component strains this can be compared with the ΔT and plotted as shown in Figure 2. It is clear that the ΔT values and the strain sum from each subset increases proportionally, with the slope of the plot being approximately 1. This is because ΔT is proportional to the stress sum, which is an invariant. Equation (1) shows that for orthotropic materials ΔT is dependent on the coupling between the stresses and the coefficient of thermal expansion. The deviation from the 1 to 1 proportionality shown in Figure 2 may be an indication of the degree of orthotropy in each subset and equivalent to the ratio of the coefficients of thermal expansion; this warrants further investigation. Whilst both imaging techniques captured variations in strain and ΔT indicating the heterogeneity of the material, the absolute magnitudes of strain and temperature changes show little correlation to surface fibre orientations and resin area fraction suggesting that much of the surface response is governed by material variations contained within the bulk.

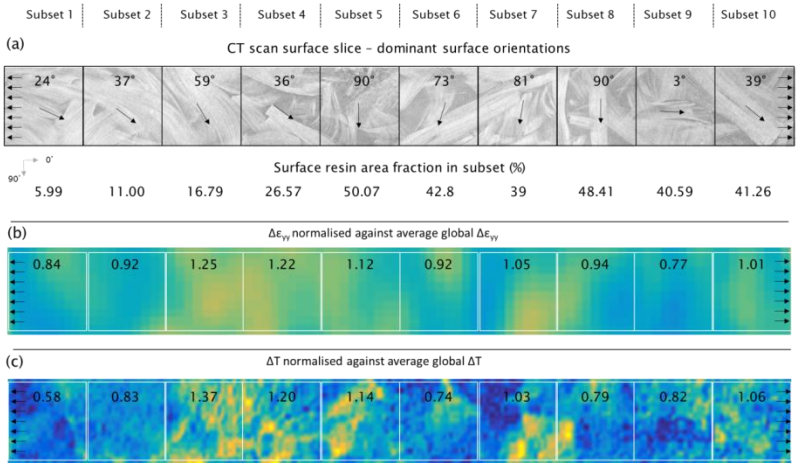

Fig 1 10 x 10 mm subsets taken from aligned (a) X-ray CT, (b) LIDIC and (c) TSA data. The dominant fibre orientation and surface resin volume fraction is quantified from CT data. This is directly compared against strain in the loading direction and temperature change in LIDIC and TSA data respectively.

Figure 3 shows the variation of ΔT and the strain sum with volume fraction, there appears to be little correlation although the scatter is not completely random and requires further investigation. A similar pattern was observed when the data was plotted against the average bulk fibre orientation contained within each subset. However Figure 4 shows that there is a correspondence between both measurements and the average ply orientation on the side of the specimen where the measurements were taken (bulk region above the mid-plane). Therefore measurements are dependent on the bulk material and change as result of local stiffness variations and localised changes in the stress/strain field resulting from the stiffness change. It is therefore clear that stiffness variations and differences in thermoelastic constant across the surface add two

competing layers of complexity when linking the ΔT response to the material stress state, and is therefore an area that requires further investigation and potential development to calibrate out the variations in the thermoelastic constant.

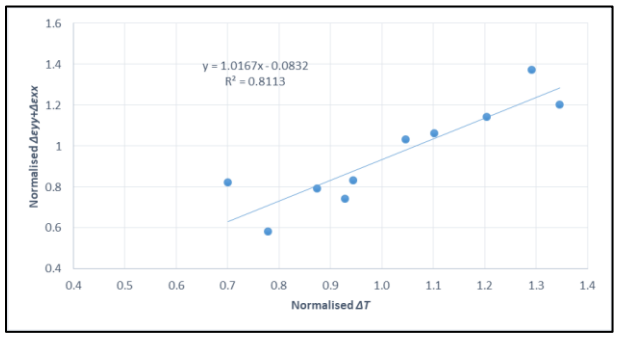

Fig 2 Comparison of LIDIC (normalised $\Delta\varepsilon_{yy}+\Delta\varepsilon_{xx}$) and TSA (normalised ΔT)

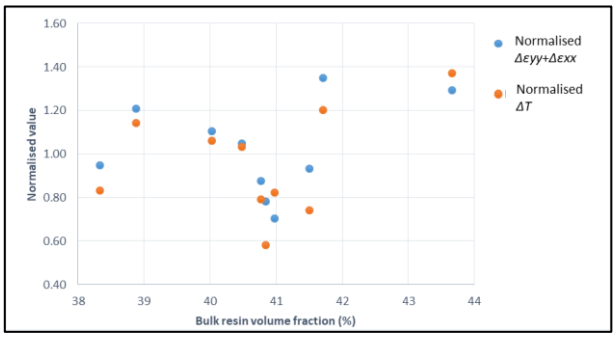

Fig 3 Comparison of surface response against the bulk resin volume fraction contained within each local subset.

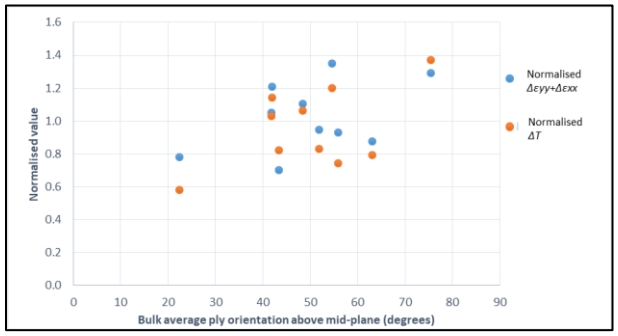

Fig 4 Surface response compared against the bulk average ply orientation within each local subset above the mid-plane (side closest to surface measurements).

Conclusions and future prospects

The work has shown that there are two competing parameters which can account for the difference between the TSA and LIDIC response: 1) variations in material stiffness resulting in a different stress and hence different temperature change for a given strain and 2) local variations in resin rich regions and local ply orientations on the surface which affects the local thermoelastic constant. In the latter case, a region with a greater resin fraction or with fibres aligned perpendicular to the loading direction would generate a higher temperature change for a given change in stress [4]. By creating data subsets and normalising against the global response these competing parameters are somewhat eliminated and it is shown that by combining the techniques there is potential to identify variations in the bulk of the material, not just at the surface and also potential to assess the degree of orthotropy in the material. By tackling the challenges highlighted in this work including calibrating the TSA response to variations in thermoelastic constants, TSA and LIDIC can be used to determine local stiffness variations and assess more complex geometries and loading configurations. The next challenge will be automating the process to help manufacturing developments and quality control.

References

1. Johanson, K., et al., *Heterogeneity of discontinuous carbon fibre composites: Damage initiation captured by Digital Image Correlation.* Composites Part a-Applied Science and Manufacturing, **68**: p. 304-312, 2015.
2. Dulieu-Barton, J.M., et al., *A temperature correction methodology for quantitative thermoelastic stress analysis and damage assessment.* Measurement Science and Technology, **17**(6): p. 1627-1637, 2006.
3. Fruehmann, R.K., et al., *The use of a lock-in amplifier to apply digital image correlation to cyclically loaded components.* Optics and Lasers in Engineering, **68**: p. 149-159, 2015.
4. Salerno, A., A. Costa, and G. Fantoni, *Calibration of the thermoelastic constants for quantitative thermoelastic stress analysis on composites.* Review of Scientific Instruments, **80**(3), 2009.